JOURNAL OF GEOPHYSICAL RESEARCH, VOL. 106, NO. C2, PAGES 2693–2712, FEBRUARY 15, 2001

What sets the mean transport through Drake Passage?

Peter R. Gent, William G. Large, and Frank O. Bryan

National Center for Atmospheric Research, Boulder, Colorado

Abstract. Twelve experiments with two coarse resolutions of a global ocean model using a variety of surface forcings are analyzed to address the question of what sets the mean transport through Drake Passage. Seven of the experiments do not have an active sea-ice model, but the remaining five do. Previous theories have suggested that the Drake Passage transport is governed by the Cape Horn Sverdrup transport or, alternatively, is proportional to the square root of the meridional Ekman transport at the latitude of Drake Passage. The results presented here do not support either of these theories. The Drake Passage transport depends quite strongly on the isopycnal diffusivity parameter in the model and less strongly on the background vertical diffusivity and horizontal viscosity parameters. However, when the magnitudes of these parameters are fixed, the results show a very strong correlation between Drake Passage transport and both the strength of the meridional Ekman transport at the latitude of Drake Passage and the thermohaline circulation off the Antarctic shelf. The relationships are monotonic, but not linear. The best estimate is that the meridional Ekman transport drives $\sim$ 100 Sv of Drake Passage transport, while the remaining 30 Sv are driven by the global thermohaline circulation.

1. Introduction

The latitude of Drake Passage, 56°S to 62°S, is unique because it is the only place in the world oceans where there is no continental barrier. This means that the dynamics should be more like the atmosphere, rather than the rest of the ocean basins. The dynamics of the Antarctic Circumpolar Current (ACC) have been discussed for nearly 50 years, since *Munk and Palmen* [1951] suggested that the lack of a barrier means that bottom topography must play a role in balancing the strong eastward wind stress at this latitude.

Despite the lack of a continental barrier, *Stommel* [1957] "suggested a theory" that the transport through Drake Passage is set by the Sverdrup transport at the latitude of Cape Horn. This transport is the integral of the curl of the wind stress right around the globe at $\sim$ 56°S. In the intervening years there have been several estimates of this Sverdrup transport from observational estimates of the wind stress and some direct monitoring estimates of the volume transport through Drake Passage. Good summaries are given in the recent papers by *Warren et al.* [1996] and *Hughes et al.* [1999]. The conclusion is that the Sverdrup and Drake Passage observational estimates are quite similar, given the error estimates, which are quite large in the case of the wind stress.

Johnson and Bryden [1989] proposed a different theory for the strength of the transport through Drake Passage. Their theory proposed that the transport is proportional to the square root of the zonal wind stress. If this stress is not constant with longitude, then the transport may be considered to be proportional to the square root of the average meridional Ekman transport at the latitude of Drake Passage.

More recently, *Krupitsky and Cane* [1994] and *Krupitsky et al.* [1996] have proposed analytic models of the ACC, in which the transport is proportional to the magnitude of the mean wind stress. In contrast, *Olbers and Volker* [1996] and *Volker* [1999] have suggested that the mean speed of the ACC is determined by nonlinear interactions between lee waves formed by bottom topography and the mean current. In this situation the ACC transport would have a very weak dependence on the wind stress.

The dynamics of the ACC has also been considered in many numerical modeling studies. A majority of these have used either simplified geometry, such as a zonal channel, or simplified physics, such as quasi-geostrophy, or a combination of the two. More recently, eddy-permitting integrations of the Southern Ocean have been carried out in a realistic geometry using the primitive equations, such as the Fine Resolution Antarctic Model (FRAM). However, these computationally expensive integrations can only be run for a few years; in

Paper number 2000JC900036
0148-0227/01/2000JC900036$09.00

the case of FRAM it was 7 years in completely prognostic mode, and so the temperature and salinity fields do not change much from their observationally based initial conditions. Figure 3 of *Hughes et al.* [1999] shows the Drake Passage transport is decreasing throughout the integration. In fact, the drift rate of the mean transport increases monotonically during the integration. Thus the FRAM integration can be used to analyze wind-driven transport fluctuations, but it would need to be integrated very much longer to reach a stable mean Drake Passage transport. This means that much coarser resolution ocean models, which can be integrated close to equilibrium, must be used to address the question of what sets the mean Drake Passage transport.

A good example of this genre of modeling study is the recent paper by *Gnanadesikan and Hallberg* [2000], who employ the global ocean model used in the earlier studies of *Toggweiler and Samuels* [1995, 1998]. The ocean domain is global, with a coarse resolution of 4.5° × 3.75° × 12 levels. The boundary conditions on temperature and salinity are restoring to observations with timescales of 30 and 120 days, respectively. They ran several cases that varied the wind stress fields forcing the Southern Ocean for 2000 years, so that they are close to equilibrium. They concluded that none of the theories discussed above give a good prediction for the Drake Passage transports found in their results. Note that all the previous theories assume that the ACC transport is constrained by the momentum balance alone. *Gnanadesikan and Hallberg* [2000] conclude that the ACC transport is determined by thermodynamics, as well as dynamics, and so depends upon the ocean heat and freshwater forcing and the strength of the thermohaline circulation.

This conclusion is consistent with earlier work by *Olbers and Wubber* [1991]. Their study uses a limited domain that has a solid boundary at 35°S and a longitude range of only 180°. The model resolution is 1.5° × 1° × 18 levels, which vary from 20 m near the surface to 500 m in the deep. They use restoring boundary conditions on temperature and salinity with a 30-day timescale. The integration is for 500 years, by which time the deep temperature and salinity had drifted away from observations, so that continuing integrations used a relaxation to observations at all depths upstream of Drake Passage in the area of 85°W to 90°W. They ran three such experiments for 50 years, which differed in the freezing rates of sea ice and hence in the magnitude of brine rejection under sea ice. The mean Drake Passage transport was sensitive to this change in the buoyancy driving off Antarctica, changing between values of 115, 130, and 160 Sv in the three experiments, as the freezing rate increased.

Cai and Baines [1996] also performed a study using a global ocean domain, with a coarse resolution of 5.6° × 3.2° × 12 levels. The boundary conditions on temperature and salinity are again restoring to observations, but with a shorter timescale of 6 days. They ran several integrations to equilibrium using the acceleration technique of *Bryan* [1984]. They show that the Drake Passage transport not only depends on the wind forcing, but also depends strongly on the ocean thermohaline forcing in the Southern Hemisphere. In addition, they found that the Drake Passage transport was quite sensitive to the values of horizontal viscosity and vertical diffusivity and to the setup of bottom topography in the ocean model. This last dependency was very clearly demonstrated earlier by *Webb* [1993]. He used both analytic and numerical models with simple geometry to show that the ACC transport depends strongly on the topography of the Kerguelen Plateau, which partially blocks the latitudes of Drake Passage. *Hughes and Killworth* [1995] discuss the sensitivity of the ACC to the bottom topography setup in the FRAM.

In this study we also use a global ocean model with fairly coarse resolutions, although they are considerably finer than those used by *Gnanadesikan and Hallberg* [2000] and *Cai and Baines* [1996]. More important, however, is that our model uses a more recent parameterization of the baroclinic effects of mesoscale eddies on model tracers and a much more realistic bulk forcing method compared to the strong restoring boundary conditions used earlier. These two upgrades have been shown to greatly improve the equilibrium fields of temperature and salt in equilibrium integrations of this type of coarse resolution ocean model [see *Danabasoglu et al.*, 1994; *Large et al.*, 1997]. This improvement has probably been largest in the high latitudes of the Southern Hemisphere and occurs in the dynamics of the ACC, in the surface heat and freshwater fluxes, and in the areas of convection that represent deep water formation. In particular, *Danabasoglu and McWilliams* [1995] show the effect of the mesoscale eddy parameterization on Drake Passage transport in a model with a resolution of 4° × 3°. Their Figure 3 shows that the Drake Passage transport reduces by 60 to 70 Sv with the eddy parameterization, compared to integrations using a horizontal Laplacian operator in the tracer equations with the same coefficient magnitude. *Danabasoglu and McWilliams* [1995, Figure 3] also show that the transport is quite sensitive to the value of the eddy parameterization coefficient, showing an approximate inverse one-third power law dependency. We believe that using the eddy parameterization in coarse resolution global models enables them to represent the unique dynamics of Drake Passage latitudes, so that they can give quantitatively realistic values of ACC transport, which is not true using horizontal tracer mixing. It is true that the Drake Passage transport in our model will depend on the topography and some of the model parameter values. However, on the basis of much previous work, we believe that the values used for the two different resolutions in this work are near the most appropriate values. We will show how the Drake Passage transport depends on some of these parameter values, but we wish

to concentrate in this paper on how changes in the way the ocean is forced change the mean transport through Drake Passage.

The layout of the paper is as follows. The ocean numerical model and the 12 experiments are documented in section 2. The 12 experiments use a variety of wind stress and buoyancy forcing from both observations and an atmospheric model and have been integrated long enough so that the transports through Drake Passage are almost independent of time. Section 3 contains a thorough analysis of three experiments that have the same resolution and curl of the wind stress forcing, but the Drake Passage transport varies by a factor of $\sim$ 2.5. Section 4 contains an analysis of the zonal momentum balance in these three experiments using our coarse resolution model. We show that this balance is consistent with observations and results from much higher resolution, eddy-permitting models. Section 5 shows results from 10 of the experiments, which vary considerably in the strengths of the wind stress and thermohaline forcings, and section 6 contains our discussion and conclusions. We conclude that the mean Drake Passage transport is not set by the Sverdrup transport at Cape Horn or by the square root of the Drake Passage meridional Ekman transport. We propose that the mean Drake Passage transport is governed by the magnitudes of eddy activity in the ocean, the meridional Ekman transport at the latitude of Drake Passage, and the thermohaline circulation off the Antarctic shelf.

2. Ocean Numerical Model

The numerical model used in this study is the ocean component of the National Center for Atmospheric Research (NCAR) Climate System Model (CSM). It is a global, full-depth configuration that uses a z coordinate in the vertical and is based on the Modular Ocean Model code 1.1. It has been upgraded to include the mesoscale eddy parameterization of *Gent and McWilliams* [1990], the new upper ocean boundary layer parameterization scheme of *Large et al.* [1994], and a third-order upwind advection scheme [see *Holland et al.*, 1998] The model has a rigid lid, uses a single vertical velocity [see *Webb*, 1995], allows transpolar flow because there is no artificial island at the north pole, and includes the additional terms in the momentum equation that ensure conservation of angular momentum [see *Wajsowicz*, 1993].

The results to be discussed in the next section have come from two different grid configurations of the model. The first configuration is the $\times 2$, which has a zonal resolution of 2.4° and a meridional grid spacing of 1.2° at the equator, increasing to 2.3° at 20°N and 20°S and decreasing to 1.2° at high latitudes. It has 45 vertical levels, with four in the upper 50 m; this configuration is described by *Gent et al.* [1998]. The second grid is the $\times 3'$, which has a zonal grid spacing of 3.6° and a meridional grid spacing of 0.9° at the equator, increasing to 3.5° at 30°N and 30°S and decreasing to 1.8° at high latitudes. It has 25 vertical levels with three levels in the upper 50 m, and is a modification of the configuration described by *Large et al.* [1997] that has halved the meridional resolution at the equator. The background vertical viscosity is 10^{-3} and 5×10^{-4} m^2 s^{-1}, and the background vertical diffusivity is 3×10^{-5} and 5×10^{-5} m^2 s^{-1} in the $\times 2$ and $\times 3'$ resolutions, respectively. The isopycnal diffusivity in the eddy parameterization is 800 m^2 s^{-1} in both resolutions, except in two experiments that are noted below. The $\times 2$ resolution uses a single, constant horizontal viscosity, with a value of 8×10^4 m^2 s^{-1}. However, the $\times 3'$ resolution uses a spatially dependent, anisotropic horizontal viscosity with different coefficients in the along-stream and cross-stream directions [see *Large et al.*, 2000]. The most important coefficient is the meridional horizontal viscosity at 55°S in the zonal momentum equation (see section 4), which is 6.9×10^4 m^{2}s^{-1}.

The results come from three different configurations of the CSM suite of models. In the first, only the ocean model is active, when a bulk forcing scheme is used that is fully described by *Large et al.* [1997]. It uses the near-surface wind speed and direction, air temperature and specific humidity from the NCAR/National Centers for Environmental Prediction (NCEP) reanalysis, solar radiation and cloud amount from the International Satellite Cloud Climatology Project (ISCCP), precipitation from Microwave Sounding Unit (MSU) satellite observations, and the model sea surface temperature (SST). Forcing with these observations also requires a bulk formula for long wave radiation that uses the model SST, near-surface air temperature and specific humidity, and ISCCP cloud amount [see *Fung et al.*, 1984]. The sea-ice distribution is diagnosed as where the *Shea et al.* [1990] SSTs are, -1.8°C, and the surface boundary conditions under sea ice are strong restoring to Levitus data. The salinity forcing includes a weak restoring to observations over the open ocean, which largely compensates for inaccurate precipitation and no river runoff [see *Gent et al.*, 1998]. The second configuration is active ocean and sea-ice models, but still using atmospheric forcing fields that come from observations or from the atmospheric component of the CSM, the Community Climate Model, version 3 (CCM3). This configuration has no restoring under sea ice, because the ocean and sea-ice interaction, such as brine rejection, is treated explicitly, and also does not have the weak, open ocean salinity restoring term. The third configuration is fully coupled CSM integrations, which use active atmospheric, land, sea-ice, and ocean models. This configuration does not use flux corrections or restoring terms in either heat or salinity. However, the ocean freshwater budget is balanced by increasing the precipitation slightly by a spatially constant factor, in order to account for the neglected river runoff [see *Boville and Gent*, 1998].

Results will be presented from 12 different integrations. Two are equilibrium, ocean-alone integrations

Table 1. Details of Integrations

Case	Res	Sea-Ice Model	Fully Coupled	Wind Forcing	Thermal Forcing	Evaporation-Precipitation Forcing	Comments	Drake Passage, Sv	Cape Horn, Sv
A	×2	no	no	NCEP 1 year	ISCCP, NCEP	MSU, NCEP	Gent *et al.* [1998]	120	139
B	×2	no	no	CCM3 5 year	CCM3	CCM3	Bryan [1998]	117	310
C	×2	yes	no	CCM3 5 year	CCM3	CCM3	Boville and Gent [1998]	250	249
D	×2	yes	no	NCEP 1 year	CCM3	CCM3	Bryan [1998]	231	85
E	×2	yes	yes	-	-	-	Boville and Gent [1998]	236	208
F	×3′	no	no	NCEP 4 year	ISCCP, NCEP	MSU, NCEP	standard parameters	134	147
G	×3′	no	no	NCEP 4 year	ISCCP, NCEP	MSU, NCEP	$\kappa_I \times 2$	91	148
H	×3′	no	no	zonal wind increased	ISCCP, NCEP	MSU, NCEP	no change in curl τ^s	241	146
I	×3′	no	no	NCEP 4 year	ISCCP, NCEP	MSU, NCEP	$\nu_H \times 1.5$	125	147
J	×3′	no	no	NCEP 4 year	ISCCP, NCEP	MSU, NCEP	$\kappa_V \times 0.6$	113	147
K	×3′	yes	no	NCEP 4 year	ISCCP, NCEP	MSU, NCEP	brine rejection	181	143
L	×3′	yes	no	NCEP 4 year	ISCCP, NCEP	MSU, NCEP	no brine rejection	122	143

NCEP, National Center for Environmental Prediction; ISCCP, International Satellite Cloud Climatology Project; MSU, Microwave Sounding Unit; CCM, Community Climate Model; κ_I, isopycnal diffusivity; τ^s, surface wind stress; ν_H, horizontal diffusivity; κ_V; background vertical diffusivity.

that have reached a stationary, repeating annual cycle for the ×2 solution or a 4-year repeating cycle for the ×3′ solution. The other integrations have been run for much shorter periods, the shortest being 25 years. However, in the two shortest integrations, the Drake Passage transport is almost independent of time, so that these short integrations have been included in this work. The equilibrium and some of the shorter integrations have been done in "accelerated" mode. This technique was introduced by *Bryan* [1984] in order to speed up the convergence to equilibrium of ocean integrations. For the ×2 integrations it consists of using a factor of 6 larger time step for the surface tracer variables than in the momentum equation and a factor of 10 larger time step for the deepest tracer variables compared to the surface tracer variables. In the ×3′ integrations, accelerated mode means the same time step for the momentum equation and surface tracer variables, but a factor of 50 larger time step for the deepest tracer variables compared to the surface variables. *Danabasoglu et al.* [1996] document how acceleration works well at these model resolutions and show that the Drake Passage transport in synchronous integrations is very close to that in accelerated mode.

The 12 integrations are now described and are listed in Table 1. The first five are older cases, using the ×2 resolution, which have been documented in previously published papers:

1. Case A is ×2 resolution, ocean alone integrated to equilibrium. This integration uses bulk forcing based on observations. The equilibrium solution is documented by *Gent et al.* [1998]. Note that the isopycnal diffusivity coefficient in this experiment is 600 $m^2\ s^{-1}$, whereas the standard value is 800 $m^2\ s^1$.

2. Case B is ×2 resolution, ocean alone integrated for 25 years in accelerated mode. This is a continuation of case A, but the atmospheric forcing fields of the bulk forcing and the radiative forcing are taken from an integration of CCM3, at the standard resolution of T42 truncation. This integration is labeled as c001.01 by *Bryan* [1998].

The three integrations that follow have an active sea-

ice model, which is the CSM cavitating fluid sea-ice model, documented by *Weatherly et al.* [1998]. They all use a value of the air to sea-ice drag coefficient that is much too large, being ~ 4 times a realistic value. This mistake was found after the integrations were completed, and the implications are discussed by *Boville and Gent* [1998].

3. Case C is $\times 2$ ocean resolution plus the cavitating fluid sea-ice model on the same grid forced by a 5-year cycle of atmospheric fields, radiation, and precipitation from an integration of CCM3 at resolution T42. This starts with the case A solution as the initial condition, is in accelerated mode for the first 50 years, and then is in synchronous mode for 10 years. This is part of the CSM spin-up procedure [see *Boville and Gent*, 1998, Figure 2].

4. Case D is another $\times 2$ ocean and cavitating fluid sea-ice integration that differs from case C in that the atmospheric forcing variables are based on observations, rather than from CCM3, but the radiative forcing still comes from CCM3. This integration is for 25 years in accelerated mode and is labeled as g006.38 by *Bryan* [1998].

5. Case E is a fully coupled CSM integration that was integrated for 300 years with no flux corrections. It is documented by *Boville and Gent* [1998], *Bryan* [1998], *Danabasoglu* [1998], and *Doney et al.* [1998]. This model comprises the CCM3, the CSM land surface model, the $\times 2$ ocean model, and the cavitating fluid sea-ice model.

The remaining seven integrations use the $\times 3'$, rather than the $\times 2$, configuration. They are recent integrations that were designed for this study, and they have not been documented before. The first five are ocean alone forced with observationally based bulk forcing.

6. Case F is $\times 3'$ resolution, ocean alone integrated to equilibrium. This integration uses a 4-year cycle of forcing, rather than the repeating annual cycle used in case A.

7. Case G is $\times 3'$ resolution ocean alone integrated with acceleration for 50 years. The difference from case F is that the isopycnal diffusivity coefficient κ_I is increased by a factor of 2 to 1600 $m^2\ s^{-1}$. Case F is used as the initial condition for case G.

8. Case H is $\times 3'$ resolution ocean alone integrated with acceleration for 50 years. The difference from case F is that the zonal wind stress is increased over the global ocean by 0.05 sec ϕ N m^{-2}, where ϕ is latitude. Note that this does not change the curl of the wind stress, and case F is used as the initial condition.

9. Case I is $\times 3'$ resolution ocean alone integrated with acceleration for 50 years. The difference from case F is that the horizontal viscosity coefficients ν_H are uniformally increased by a factor of 1.5. Case F is used as the initial condition for case I.

10. Case J is $\times 3'$ resolution ocean alone integrated with acceleration for 50 years. The difference from case F is that the background vertical diffusivity κ_V is decreased from 5×10^{-5} to 3×10^{-5} $m^2\ s^{-1}$. Case F is used as the initial condition for case J.

The remaining two integrations do have an active sea-ice model, but use the viscous-plastic rheology of *Zhang and Hibler* [1997]. However, the same thermodynamics as the cavitating fluid sea-ice model are used. The integrations also use a much smaller and realistic value of the air to sea-ice drag coefficient than that used in integrations C-E.

11. Case K is $\times 3'$ resolution ocean with the viscous-plastic sea-ice model and observationally based bulk forcing. The integration is for 50 years in accelerated mode, using case F as the initial condition.

12. Case L is $\times 3'$ resolution ocean and viscous-plastic sea-ice model again forced as in case K, except that brine rejection has been switched off by setting the salinity of sea ice to be the same as that of the ocean. The integration is for 50 years in accelerated mode, using case F as the initial condition.

3. No-Curl Change Experiments

In this section, experiments F, G, and H are analyzed in detail. Case F is a recent version of our coarse resolution configuration, which has been integrated for a very long time of 15,000 deep ocean tracer years. This means that it is very close to equilibrium and has a repeating 4-year cycle, as do the forcing fields. In experiment G the isopycnal diffusivity coefficient has been changed, because the ACC transport is most sensitive to this mixing coefficient. Figure 3 of *Danabasoglu and McWilliams* [1995] shows an approximate inverse one-third power law dependency. Experiment H is discussed as a "thought experiment" by both *Warren et al.* [1996] and *Hughes* [1997]; the strength of the zonal wind stress is increased, without changing the wind stress curl. Cases G and H were specifically designed so that the curl of the wind stress is unchanged from case F. This has not been achieved exactly in these cases; only to about 0.8%, because the drag coefficient has a weak dependence on model SST. Thus only if there is no change in the SST distribution will the wind stress remain exactly the same.

The result of averaging the barotropic stream function from the last 4 years of case F is shown in Figure 1. The average transport through Drake Passage in this case is 134 Sv, and the Sverdrup transport at the latitude of the model Cape Horn (55.8°S)calculated from the curl of the wind stress is 147 Sv. The Drake Passage transport in this experiment is consistent with the real-world value suggested by observations, which is 130 $\pm$ 13 Sv [see *Whitworth et al.*, 1982; *Whitworth*, 1983]. The curl of the wind stress at Cape Horn from the NCEP reanalyzed atmospheric surface winds is not inconsistent with previous estimates, because the error bars on this type of calculation are usually large. We also note that there is a rather strong meridional gradient in the Sverdrup transports calculated from the

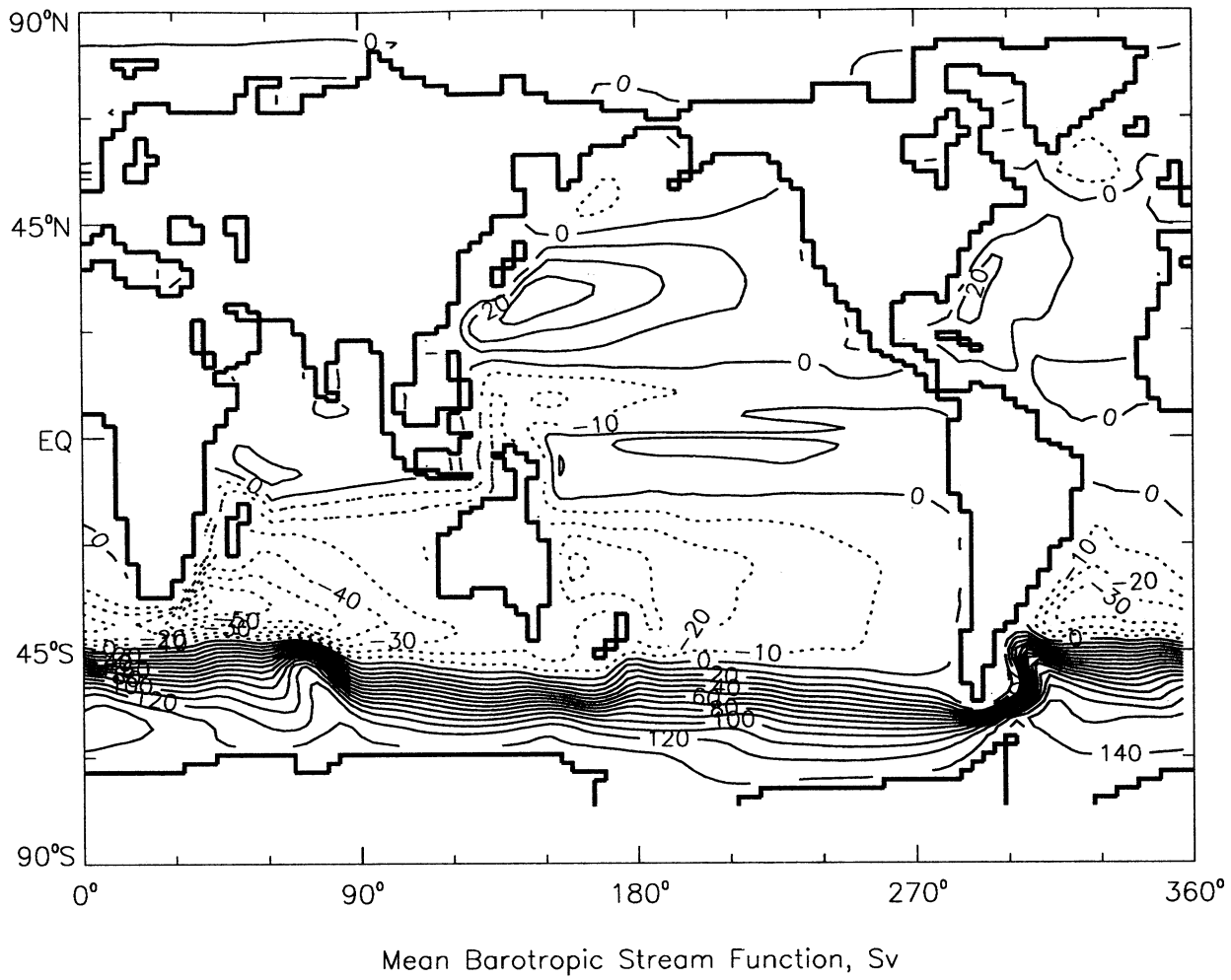

Figure 1. Annual mean barotropic stream function from case F, 4-year average. The contour interval is 10 Sv.

NCEP reanalysis between 50°S and 60°S. The Sverdrup transports half a grid point north and south of Cape Horn are 124 Sv at 54.9°S and 170 Sv at 56.7°S. However, the results from case F do not contradict the hypothesis that the mean Drake Passage transport is set by the Sverdrup transport at the latitude of Cape Horn.

The second stream function that is standardly shown from ocean circulation models is the meridional overturning stream function. With the *Gent and McWilliams* [1990] mesoscale eddy parameterization, however, there are two meridional stream functions. The first is derived from the effective transport velocity, which is advecting potential temperature and salinity, and is shown in Figure 2a from case F. The second uses the Eulerian mean velocity, which advects velocity, and this overturning stream function from case F is shown in Figure 2b. The figure clearly shows that the cell due to the Eulerian velocity located between 45°S and 60°S, which is often called the Deacon cell, is considerably weaker in Figure 2a in the depth range of 0.5 to 3 km. This results from the overturning circulation due to the parameterized eddies opposing that due to the mean flow in this region. This does not happen near the ocean surface, because the eddy transport tapers toward zero in the upper ocean mixed layer. Overall, this is a rather faithful representation of what mesoscale eddies do in ocean integrations with a horizontal resolution that permits a reasonable level of eddy activity [see e.g., *Doos and Webb*, 1994; *Killworth and Nanneh*, 1994]. The second reason that the *Gent and McWilliams* [1990] mesoscale eddy parameterization works well in the ACC region is that false diapycnal mixing due to horizontal mixing of potential temperature and salinity has been eliminated. The mixing of potential temperature and salinity is now along isopycnals. This parameterization results in weaker transports of heat and fresh water across the ACC and more realistic surface fluxes south of the ACC [see *Danabasoglu et al.*, 1994; *Gent et al.*, 1995].

The mean barotropic and meridional overturning stream functions from case G are shown in Figures 3 and 4, respectively. Figure 3 shows that doubling the coefficient of isopycnal diffusivity to 1600 m^2 s^{-1} reduces the Drake Passage transport from 134 to 91 Sv. This is a

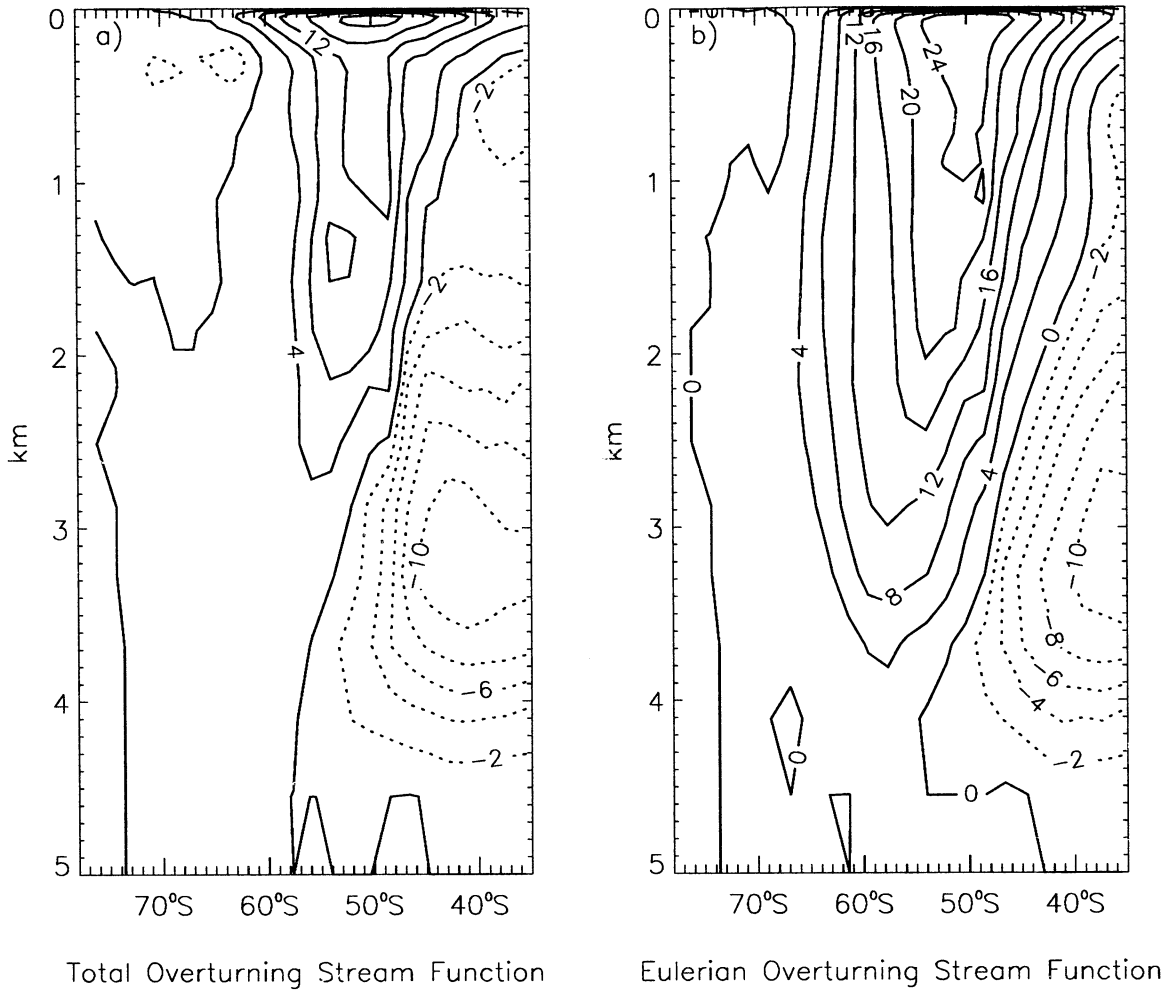

Figure 2. Annual mean meridional overturning stream function based on (a) the effective transport velocity and (b) the Eulerian mean velocity from case F. The contour interval is 4 Sv for positive values and 2 Sv for negative values.

reduction of > 30%, while the Sverdrup transport at the latitude of Cape Horn has increased very slightly from 147 to 148 Sv. Also note from Figure 3 that the barotropic transports, except for the ACC, are hardly changed at all compared with those in case F, which are shown in Figure 1. In zonally bounded ocean basins the linear dynamics in this coarse resolution model means that the midlatitude gyre transports are set by the Sverdrup transport, a result shown previously by *Danabasoglu* [1998]. Figure 4 shows that the Eulerian meridional overturning stream function is not changed very much between the two experiments, but the effective transport has been reduced considerably in case G compared with case F. In case G there is a much reduced area of positive values between 50°S and 60°S and 1 to 3 km.

This last fact is the clue to what has happened in case G, which would have twice as strong eddy-induced velocities as case F if the density field were unchanged. *Gent et al.* [1995] show that the eddy-induced circulation simulates baroclinic instability by flattening the model isopycnals and reducing the potential energy. At the start of case G this happens at twice the previous rate and continues until a new equilibrium is reached with reduced meridional density gradients in the ACC. This is illustrated in Figure 5, which shows the zonally averaged σ_θ between 35°S and 78°S for case F and for the difference between case F and case G. Figure 5b shows that the density in case G is increased (decreased) to the north (south) of the ACC above 2.5 km. Below 2.5 km the density changes are larger in the south than in the north. This implies a flattening of the isopycnals everywhere between 35°S and 78°S in case G compared with case F. By geostrophy this implies reduced vertical shears of zonal velocity. Small zonal velocities in the deep ocean then imply smaller zonal velocities throughout the water column and hence a reduced barotropic transport. This is shown in Figure 6, which is a plot of the zonally averaged zonal velocity against depth at 57.7°S and 59.6°S, which are two latitudes corresponding to the model Drake Passage. Figure 6 shows that the average zonal velocities in case G are smaller than

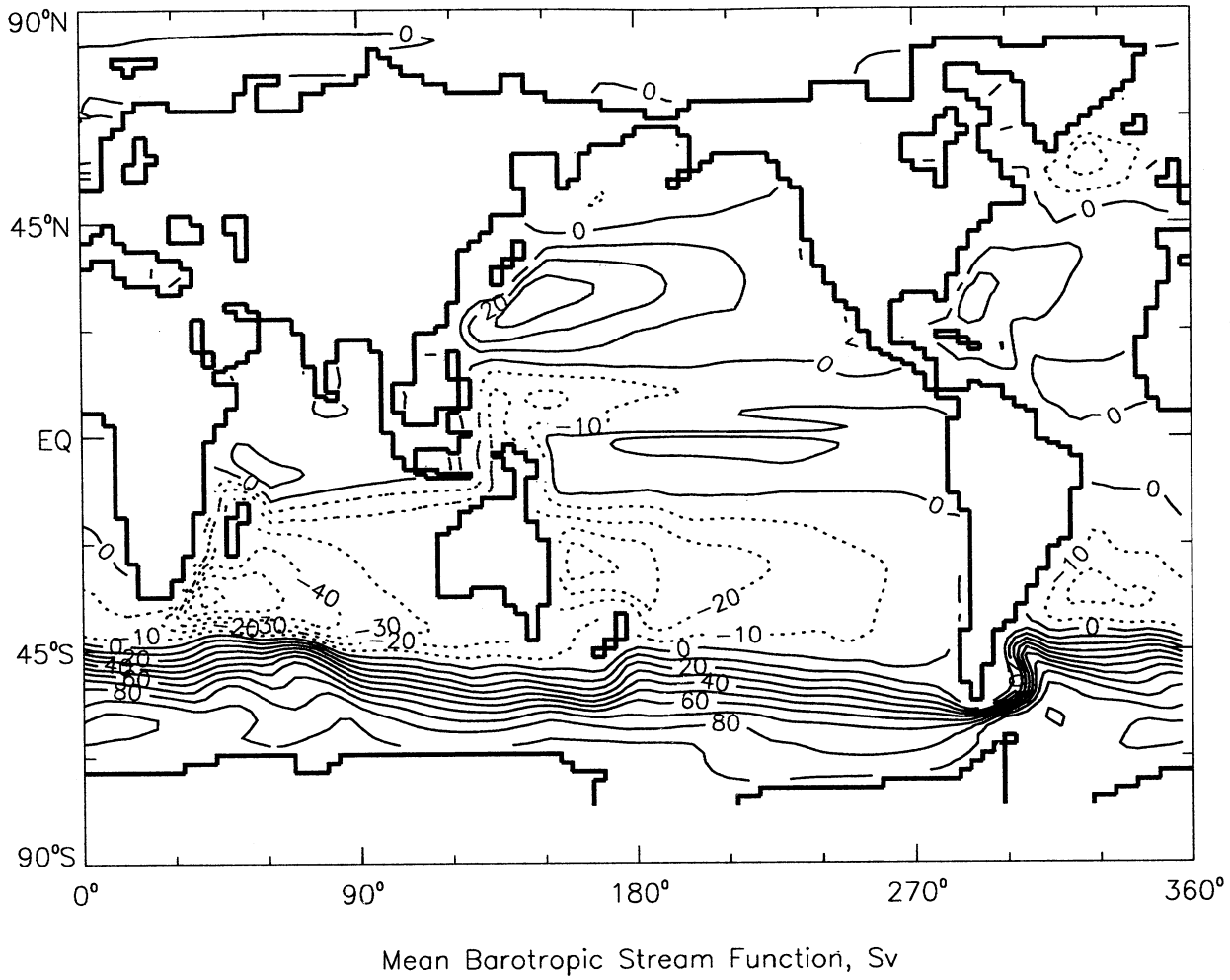

Figure 3. Same as Figure 1, but from case G.

those in case F throughout the water column. It also shows the averaged zonal velocities from case H, which we discuss next.

The difference between cases H and F is that an additional zonal wind stress of 0.05 secϕ N m^{-2}, where ϕ is latitude, has been added. The secϕ distribution ensures that this additional stress has zero curl in spherical coordinates. At the latitude of Drake Passage, 60°S, the additional wind stress is 0.1 N m^{-2}, while at the equator it is 0.05 N m^{-2}, which means that the mean zonal wind stress is close to zero in the equatorial Pacific Ocean. North of 70°N, the additional wind stress is constant with latitude because secϕ is getting large there, but this affects only the circulation in the Arctic Ocean. The mean barotropic and meridional overturning stream functions from case H are shown in Figures 7 and 8, respectively. Figure 7 shows that the Drake Passage transport increased sharply to 241 Sv from 134 Sv in case F, while the Sverdrup transport at the latitude of Cape Horn is essentially unchanged at 146 Sv. Figure 7 also shows that the transports of the midlatitude gyres have hardly changed in case H compared with those in case F, shown in Figure 1, because they are set by the curl of the wind stress. Figure 8 reflects the much stronger Ekman transport in the Southern Hemisphere in case H than in case F. The maximum meridional transport near the surface at 50°S in case H is 38 Sv, compared with the value of 22 Sv in case F, shown in Figure 2. This increase is all in the Eulerian mean overturning, because the eddy-induced circulation is very small in the upper 50 m. This means that the return southward transport below the Ekman layer must be stronger in case H than in case F. Figure 8 shows that, at the latitude of Drake Passage, most of this stronger southward return flow occurs below 2.3 km, which is the minimum depth of the topography. However, a small amount of the increased southward flow occurs above the topography, which can be seen by comparing the Coriolis terms in Figure 9b and Figure 10b. Throughout the ocean interior this stronger Coriolis force causes a positive acceleration of the zonal velocity and hence a stronger ACC. It is this acceleration that causes the larger zonal velocities in case H shown in Figure 6. In our model this acceleration stops

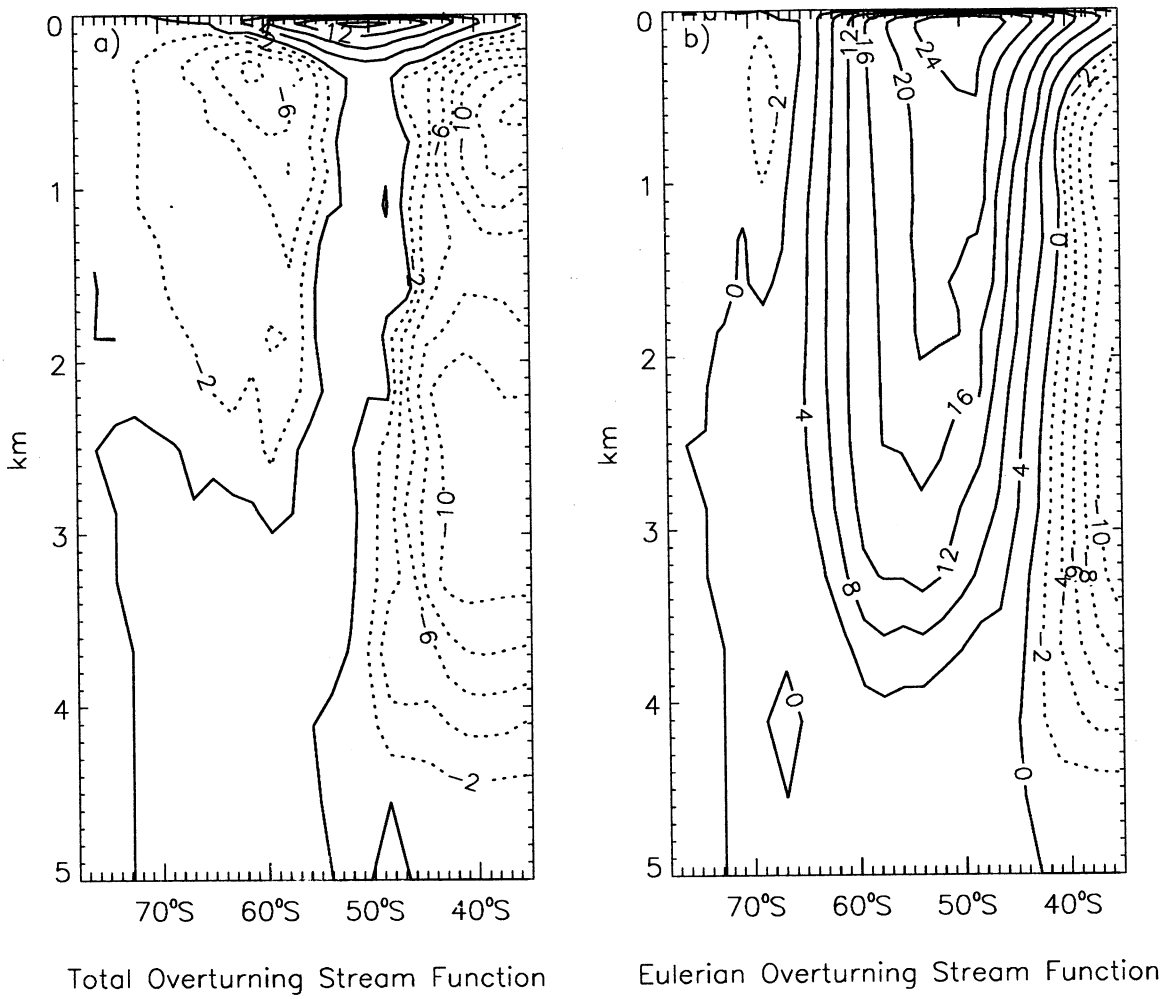

Figure 4. Same as Figure 2, but from case G.

when the force balance is restored with the larger zonally averaged Coriolis force balanced by a larger parameterized meridional viscosity term. This force balance in the zonal momentum equation for these three experiments will be examined in detail in the next section.

Experiment H is discussed as a thought experiment by both *Warren et al.* [1996] and *Hughes* [1997]. Warren et al. suggest that the Drake Passage transport will not change because the curl of the wind stress is unchanged, whereas Hughes anticipates an increase in the ACC. In experiments F, G, and H, the Sverdrup transport at the latitude of Cape Horn is constant to within 1%, but the Drake Passage transports vary by a factor of ~ 2.5, from 91 to 241 Sv. This clearly demonstrates that, in our model, the Drake Passage transport is not set by the Sverdrup transport at Cape Horn.

Experiment G shows how the ACC transport varies with the magnitude of the isopycnal diffusivity; does it depend on the other mixing coefficients? Two further experiments have been run to explore this question. In case I the horizontal viscosity coefficients in the $\times 3'$ resolution have been multiplied by a factor of 1.5 compared with case F. After 50 years in accelerated mode, the Drake Passage transport has changed from 134 to 125 Sv. In case J the background vertical diffusivity has been reduced from 5 to 3×10^{-5} m^2 s^{-1}, which is the standard value in the $\times 2$ resolution. After 50 years in accelerated mode, the Drake Passage transport has also declined from 134 to 113 Sv. These dependencies are not small, but are not as large as those on isopycnal diffusivity. Other integrations (not listed) have shown that the ACC transport is almost independent of the background vertical viscosity value, but is dependent on the exact setup of the bottom topography. It depends on how much the topography is smoothed and on the exact choice of the sill and plateau depths, which are always kept as close to reality as the vertical resolution allows.

In setting up the ocean component of the CSM, we ran many cases varying the mixing coefficients and the bottom topography setup. Our experience is that the ACC transport in different resolutions varies considerably less than might be expected from experiments such as I and J, where one parameter is changed at a fixed resolution. The reason is that going from the $\times 3'$ to the $\times 2$ resolution, for example, the vertical resolution

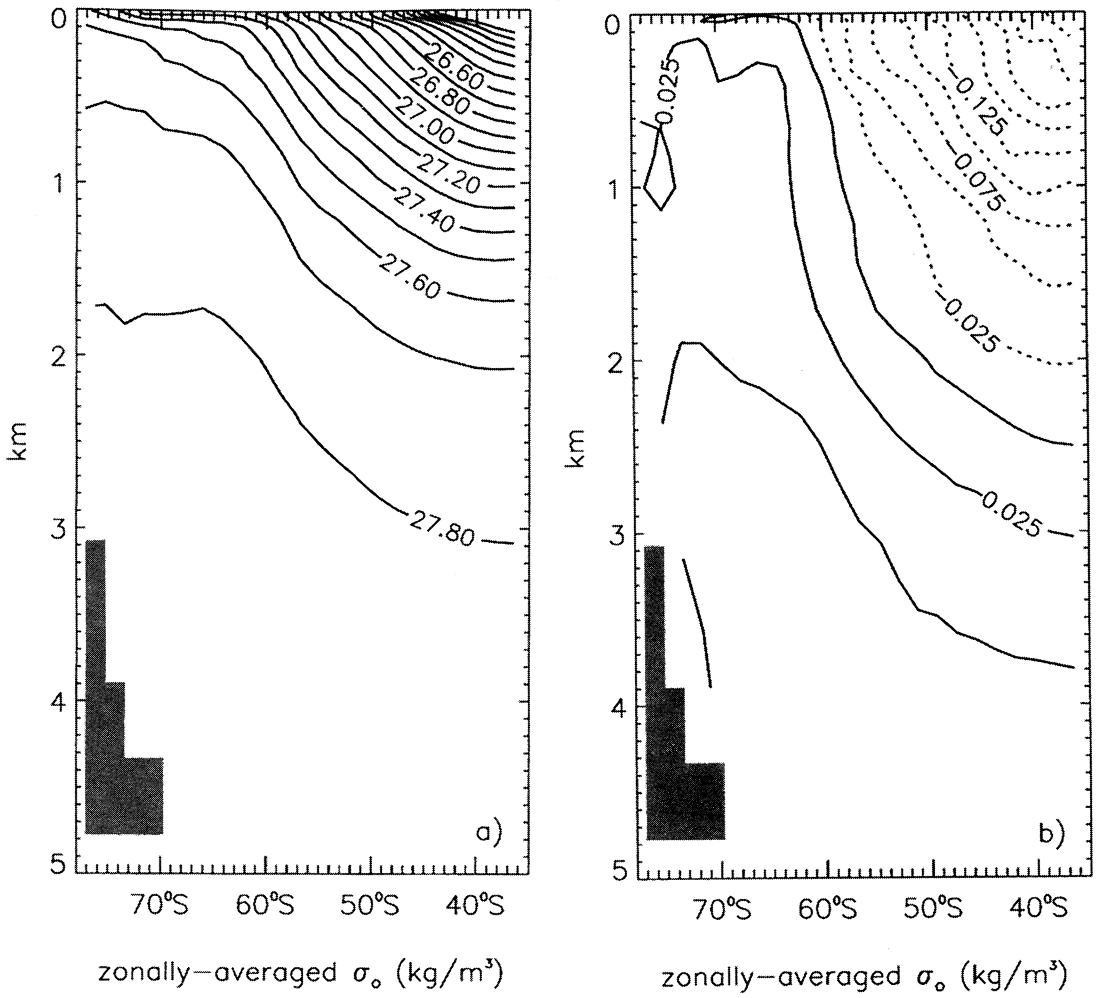

Figure 5. Zonally averaged σ_0 (in kg m^{-3}) between 35°S and 80°S for (a) case F and (b) case F - case G.

is also increased, so that both the horizontal viscosity and background vertical diffusivity coefficients can be decreased and the bottom topography can be less smooth. The effects of these changes on the ACC transport cancel to a large degree, so that transport values in the $\times 3'$ and $\times 2$ resolutions are not too different. We believe that the parameter choices used in the two different resolutions are near the most appropriate values. In this work we wish to concentrate on how changes in the way the ocean is forced change the Drake Passage transport, rather than completing an exhaustive parameter sensitivity study.

4. Model Zonal Momentum Balance

In this section we examine the balances in the zonal momentum equation and show that the balance in our coarse resolution model is consistent with what has been diagnosed in much higher resolution, eddy-permitting simulations of the ACC. Section 6 of *Olbers* [1998] summarizes the zonal momentum balance of the ACC in high-resolution simulations using both quasi-geostrophic models and primitive equation models, such as FRAM. Olbers divides the zonal momentum balance of the ACC into three different depth regions: the Ekman, intermediate, and deep layers.

We have evaluated all the terms in the zonally integrated zonal momentum equation time averaged over the last 4-year forcing cycle. The time derivative, vertical advection, and metric terms are so small that they have been ignored in the analysis presented below. The remaining terms in the zonally integrated zonal momentum equation of our model in spherical coordinates are

$$< (vu\cos\phi)_\phi/a\cos\phi > - < fv >= \Sigma\, \delta p/a\cos\phi + < (\nu_H u_\phi \cos\phi)_\phi/a^2\cos\phi > + < \tau_z > . \quad (1)$$

Angle brackets denote a complete zonal average, u and v are zonal and meridional horizontal velocities, a is the mean Earth's radius, and f is the Coriolis parameter. The pressure term represents the contribution to the momentum balance by pressure differences, δp, across ocean basins. At the latitude of Drake Passage, where

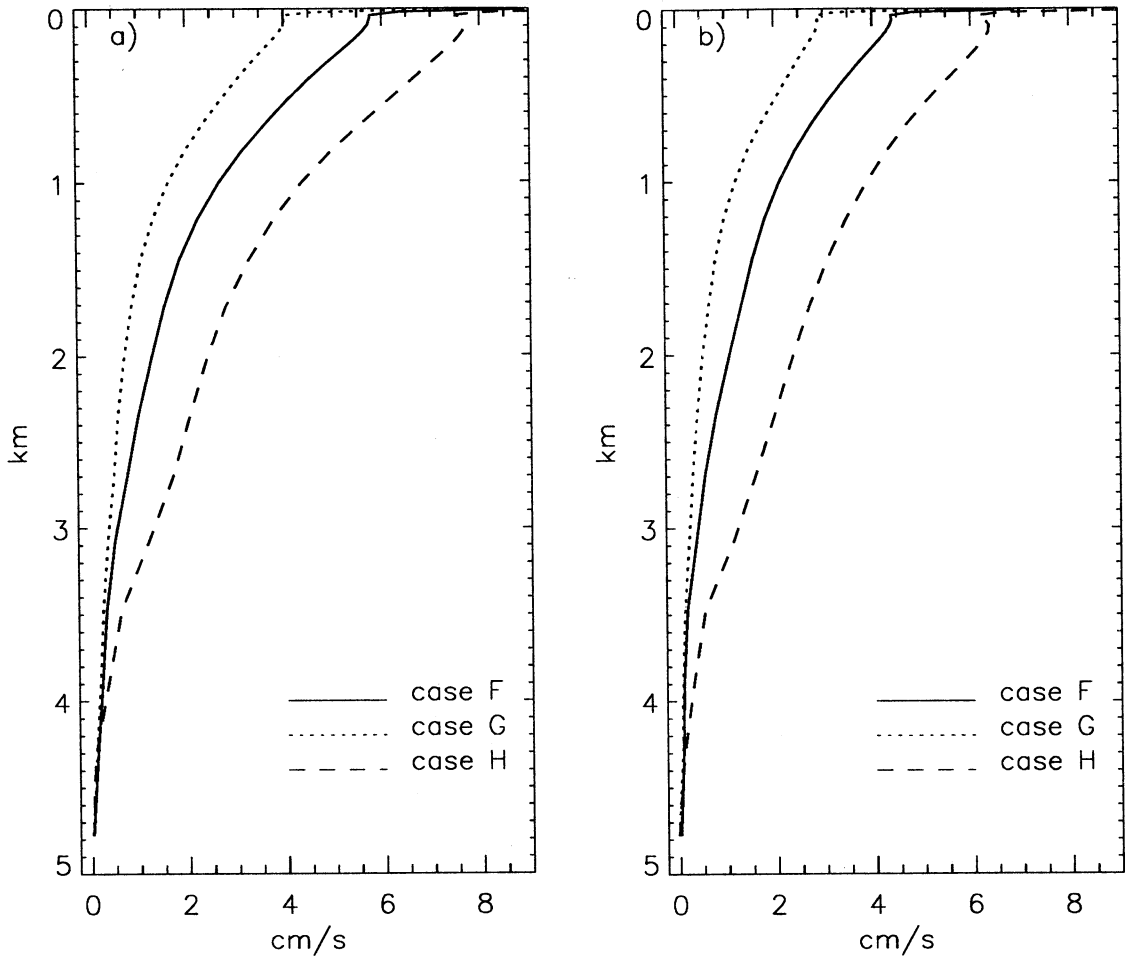

Figure 6. Zonally averaged zonal velocity (in cm s^{-1}) from cases F, G, and H at (a) 57.7°S and (b) 59.6°S.

there are no continents, it represents the pressure differences between topographic ridges in the deep ocean. Note that in our coarse resolution model, the eddy contribution to the inertial term is parameterized as the Laplacian meridional viscosity term, with coefficient ν_H, on the right-hand side of (1). The last term on the right-hand side of (1) is the vertical divergence of the frictional stress, τ. The balance of terms at latitude 57.7°S in case F averaged over the last 4 years of the integration in the Ekman, intermediate, and deep layers is shown in Figures 9a, 9b and 9c, respectively.

The first of the regions defined by *Olbers* [1998, p. 1651] is the Ekman layer, which he defines as "depths directly influenced by the wind stress." Here the dominant balance is between the Coriolis force and the vertical divergence of the frictional stress. Figure 9a shows that this is also the dominant balance in the upper model layers above 80 m. The magnitude of the Coriolis and stress terms at 20 m is $\sim 2.5 \times 10^{-4}$ cm s^{-2}, corresponding to a maximum northward velocity of 2 cm s^{-1}. The vertical extent and structure of the Ekman layer in the model is determined by the K-profile parameterization (KPP) boundary layer parameterization, which has been shown by *Large et al.* [1994] to give very realistic boundary layer depths. The next largest term in the Ekman layer is the meridional viscosity, but above 40 m it is 2 orders of magnitude smaller than the dominant terms.

Olbers [1998] calls the second region the intermediate layer, which is below the Ekman layer but above the minimum depth of the topography. Here [*Olbers*, 1998, p. 1651] "the balance is between the lateral Reynolds stress divergence and the Coriolis force," with the remaining terms being much smaller. "The dominant terms are, however, more than two orders of magnitude smaller than the dominant terms in the Ekman layer" [*Olbers*, 1998, p. 1651]. The zonal momentum balance between 100 m and 2 km at 57.7°S from the model is shown in figure 9b. Below 200 m the balance is between the Coriolis force due to the southward flow and meridional viscosity. Between 400 m and 2.4 km the magnitude of these two dominant terms is $< 2 \times 10^{-6}$ cm s^{-2}, which is almost exactly 2 orders of magnitude smaller than the dominant terms at 30 m in the middle of the Ekman layer. Figure 9b also shows that the vertical stress term is an order of magnitude smaller

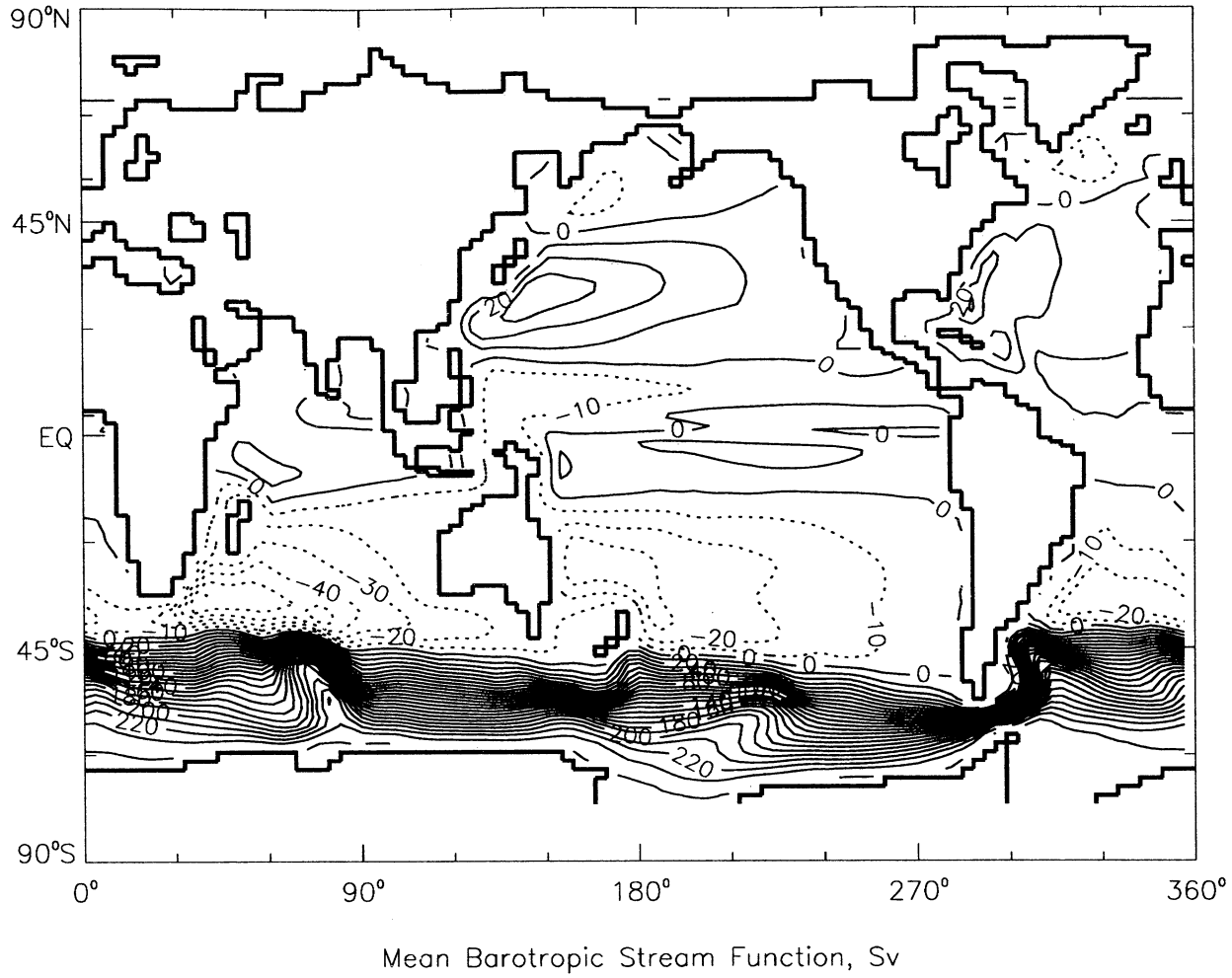

Figure 7. Same as Figure 1, but from case H.

than the dominant terms below 150 m, and is negligible below 400 m.

The third region defined by *Olbers* [1998, p. 1652] is the deep layer, which is "at depths where the topography interrupts the circumpolar path," so that the pressure term can be nonzero. In this region the dominant balance is between the pressure term and the Coriolis force, and [*Olbers*, 1998, p. 1652] "the two terms are of the same magnitude as the terms in the Ekman layer". Figure 9c shows the zonal momentum balance in the model below 2 km. Below 2.3 km the bottom pressure term almost exactly balances the Coriolis term, which is due to the strong meridional flow to the south. In the deep layer the dominant terms have a magnitude of 10^{-5} cm s^{-2}, which is a factor of 5 larger than the dominant terms in the intermediate layer but more than an order of magnitude smaller than the dominant terms in the model Ekman layer. However, the deep layer is $\sim$ 2 km deep, which is more than an order of magnitude deeper than the Ekman layer. Integrals of the southward and northward velocities in these layers match closely, with the small residual southward flow occurring in the intermediate layer.

Figure 9 shows that the zonal momentum balance in our model is almost exactly that described in section 6 of *Olbers* [1998], which was based on results from eddy-permitting ocean models. The only difference is the magnitude of the dominant terms in the deep layer. This increases our confidence in the results obtained from our coarse resolution model, where the eddy inertial term is parameterized by meridional viscosity. We also note that the Drake Passage transport is relatively insensitive to the value of horizontal viscosity, with case I showing a 9 Sv decrease when the horizontal viscosity is increased by 50%.

The corresponding zonal momentum balance at 57.7°S from case H is shown in Figure 10. The dominant balances in the Ekman, intermediate, and deep layers are exactly the same as described for case F. Comparing Figures 9b and 10b, however, shows that the vertical stress term in case H does not become negligible until 700 m, compared with 400 m in case F. However, in this depth range it is still an order of magnitude smaller than the Coriolis and meridional viscosity terms. Figures 9c and 10c show that most of the increased Ekman transport in case H is returned southward between 2.7

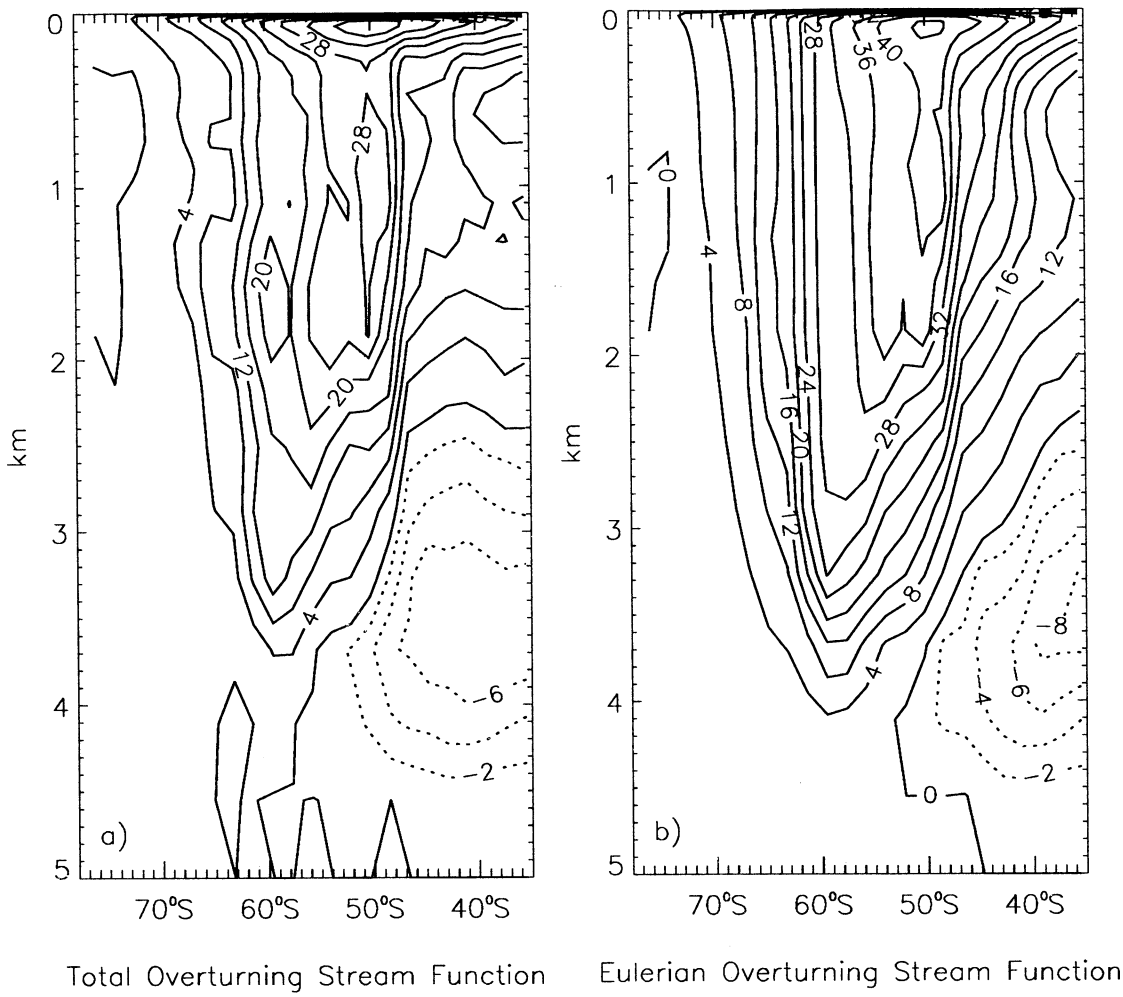

Figure 8. Same as Figure 2, but from case H.

and 3.5 km, which is below the highest topography at 57.7°S. Figures 9b and 10b show that the southward flow throughout the intermediate layer is also slightly increased in case H compared with case F. This requires a larger lateral Reynolds stress divergence in this layer in case H, which is provided by a stronger zonal velocity (see Figure 6), and this increases the ACC transport. Our hypothesis is that the mean Drake Passage transport is mostly set by the strength of the southward meridional flow in the intermediate layer, and this will be discussed in the next section.

5. Drake Passage Transport Results

Previous Drake Passage transport theories are discussed in the Introduction. Is the strength of the Drake Passage transport set by the Sverdrup transport at the latitude of Cape Horn? Figure 11 is a plot of the Cape Horn Sverdrup transport against the Drake Passage transport from 10 of the experiments. Several experiments have values close to the diagonal on Figure 11: cases A, C, F, and L. However, cases B and D have values that are very far from the diagonal. Both these experiments are described by *Bryan* [1998]. Case B uses the wind stress forcing from the standard climatological integration of CCM3. This wind stress is somewhat larger than observations in the ACC latitudes, and the maximum is shifted slightly northward. This gives rise to a large increase in the Sverdrup transport at Cape Horn because of the very large meridional gradient in this transport at these latitudes [see *Danabasoglu*, 1998]. However, the Drake Passage transport is virtually unchanged in this case from case A, which used observed wind stresses. In case D the westerlies are shifted a little to the south, compared with case A, which reduces the Cape Horn Sverdrup transport somewhat to 85 Sv. However, the Drake Passage transport is quite large at 231 Sv. Note that case D has an active sea-ice model, which results in a significantly stronger thermohaline circulation in this experiment than in cases A and B.

All the $\times 3'$ experiments, F-L, have almost the same Cape Horn Sverdrup transport; experiments G-J were discussed in section 3. Experiments K and L use the same forcing fields and ocean model parameter values as case F, but they have an active sea-ice model with and without brine rejection turned on. The sea-ice model

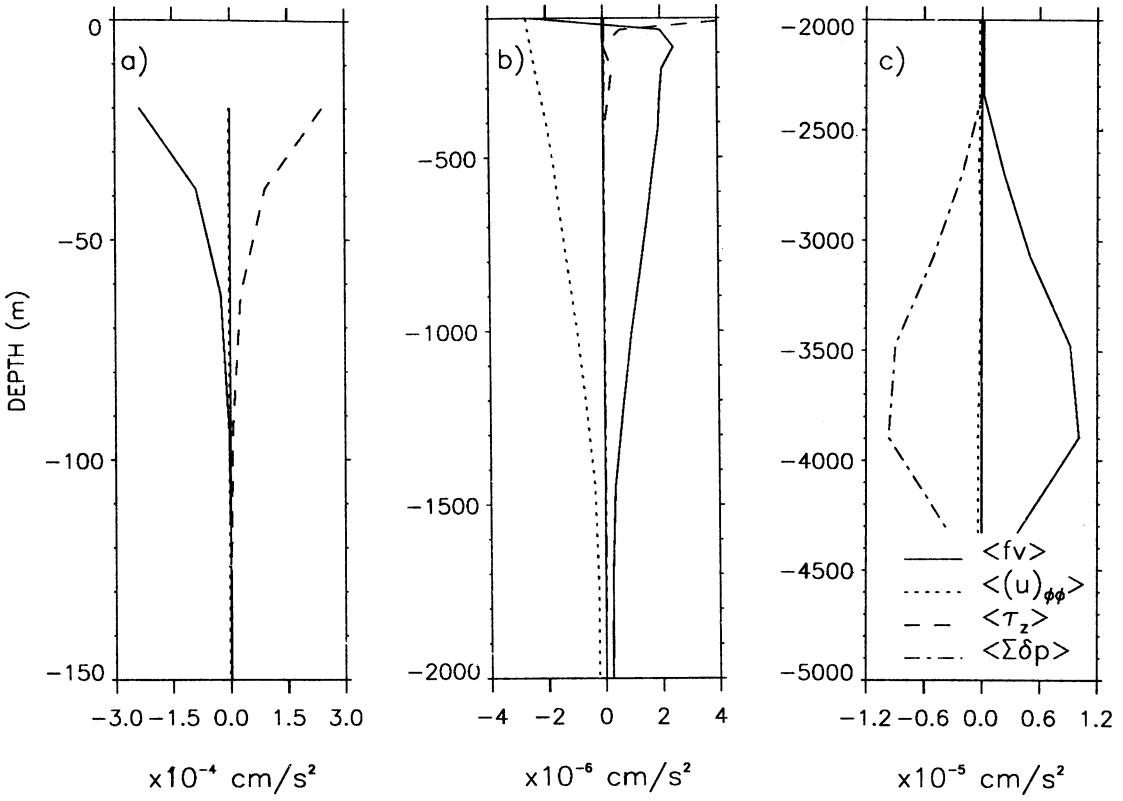

Figure 9. Balance of terms in the zonally integrated zonal momentum equation at 57.7°S (in cm s^{-2}) from case F in (a) the Ekman layer, (b) the intermediate layer, and (c) the deep layer.

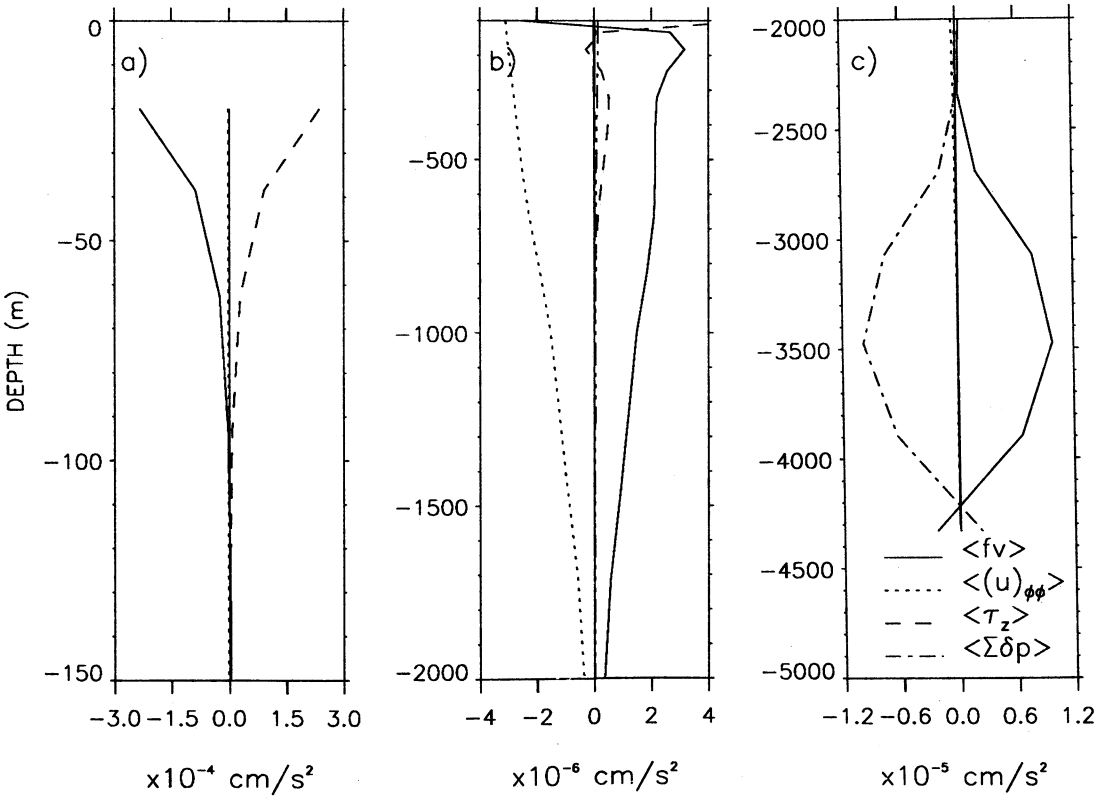

Figure 10. Same as Figure 9, but for case H.

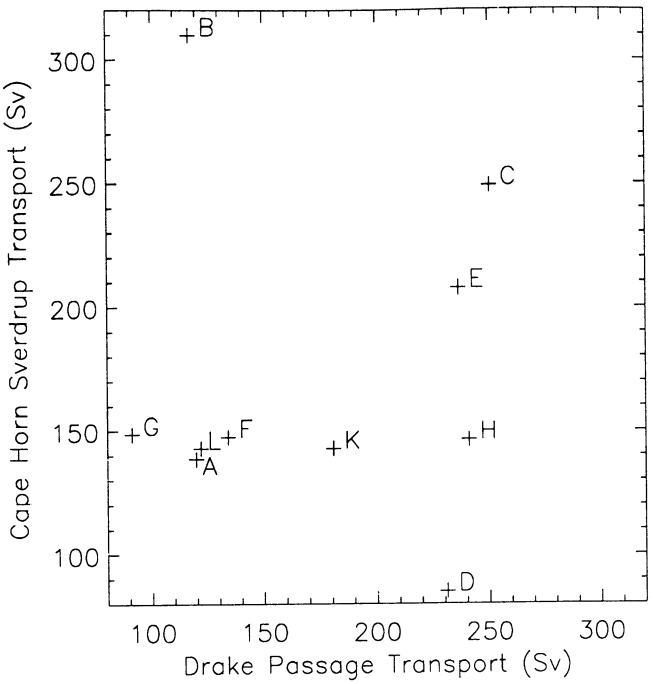

Figure 11. Cape Horn Sverdrup transport (in Sv) against Drake Passage transport (in Sv) from 10 of the model experiments.

with brine rejection has a large effect on the Drake Passage transport, increasing it to 181 Sv in case K from 134 Sv in case F, which does not have an active sea-ice model. We conclude from Figure 11 that the mean Drake Passage transport is not set by the Sverdrup transport at Cape Horn.

Johnson and Bryden [1989] assumed that the wind-driven zonal momentum is carried down by eddy processes to depth, where it can be removed by bottom pressure differences across ridges. After making assumptions about the eddy field and its transport, they concluded that the strength of the ACC is proportional to the square root of the meridional Ekman transport averaged over the latitude band of Drake Passage. Figure 12 is a plot of this quantity against the Drake Passage transport from nine of the model experiments. It shows that case H, with the considerably stronger zonal wind stress, does drive a very strong Drake Passage transport of 241 Sv. However, similarly large Drake Passage transports occur in cases C-E, and these are the experiments with the very strong thermohaline circulations because of the much too large air to sea-ice drag coefficient. We conclude from Figure 12 that the Drake Passage transport in our coarse resolution model is not set by the square root of the meridional Ekman transport.

We believe that the Drake Passage transport is mostly set by the magnitude of the southward transport in the intermediate layer of the ocean at the latitude of Drake Passage. The reason is that the resulting Coriolis force has to be balanced, and in our model this is accomplished by the lateral Reynolds stress divergence. As diagnosed in section 4, this sets the zonal velocity in the intermediate layer and hence a large part of the ACC transport (see Figure 6). Figure 13 shows the difference between the maximum and minimum values of the meridional overturning stream function based on the effective transport velocity at 61.5°S plotted against Drake Passage transport from nine of the model experiments. In order to use only standard parameter values for this figure, experiments G, I, and J have been omitted. Figure 13 shows a very strong correlation between these two quantities, giving support to our hypothesis. This southward transport in the intermediate layer is set by two main factors. The first is the strength of the meridional Ekman transport at the latitude of Drake Passage, and the second is the strength of the thermohaline circulation off Antarctica. The evidence for the dependence on the meridional Ekman transport is discussed in sections 3 and 4, mostly from comparing experiments F and H (see Figures 9 and 10).

We now show how the strength of the thermohaline circulation off Antarctica affects the southward transport in the intermediate layer. Experiments C-E have very strong thermohaline circulations, and Figure 14a and Figure 14b show the effective transport and Eulerian mean meridional overturning stream functions, respectively, averaged over the last 5 years of experiment C. Figure 14a shows that most of the deep water formed off the Antarctic shelf flows northward below 3 km depth. This increased northward transport has to

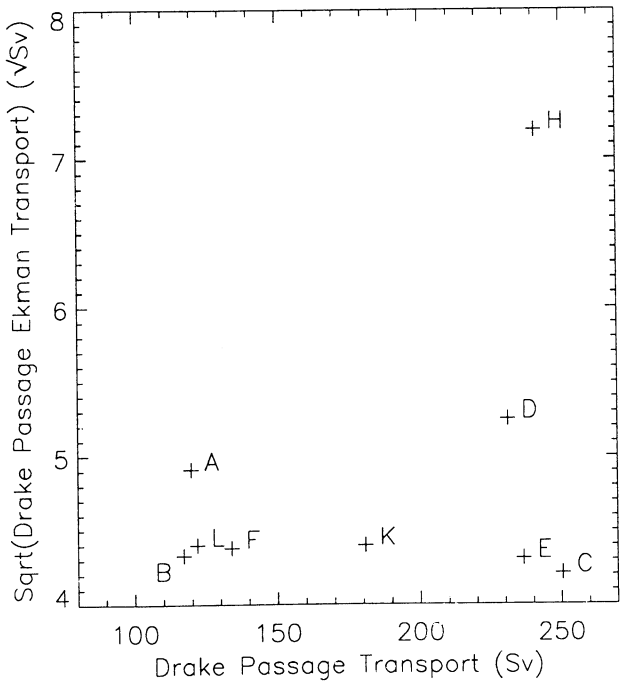

Figure 12. Square root of the Ekman transport averaged over Drake Passage latitudes (in $(Sv)^{1/2}$) against Drake Passage transport (in Sv) from nine of the model experiments.

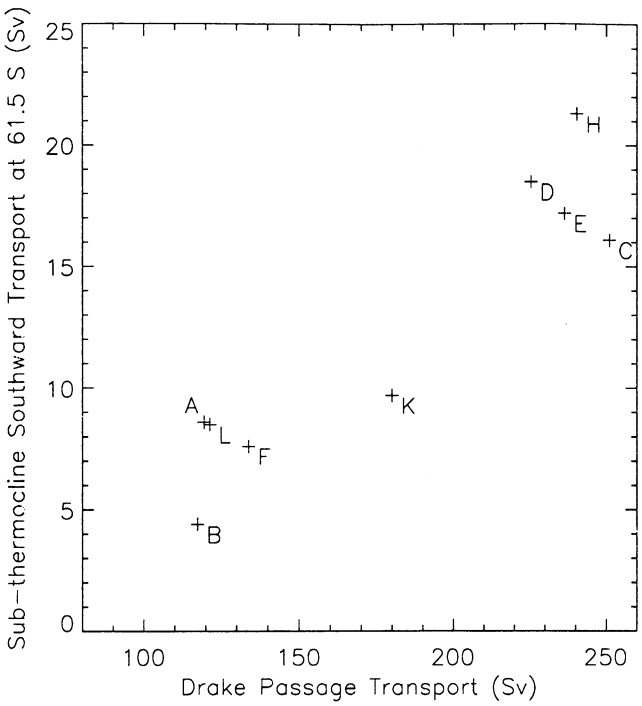

Figure 13. Difference between the maximum and minimum values of the meridional overturning stream function based on the effective transport velocity at 61.5°S (in Sv) against Drake Passage transport (in Sv) from nine of the model experiments.

be compensated by stronger southward transport above 3 km, and some of this transport occurs in the intermediate layer, which occupies the depth range from 400 m to 2.3 km.

A measure of the strength of the thermohaline circulation is the minimum in the meridional overturning stream function shown in Figure 14a, south of 65°S in the upper 2 km of the ocean. We note that this is only an approximate measure, because the effective transport velocity includes the parameterized effect of mesoscale eddies but does not include the effect of standing eddies. Figure 15 is a plot of this measure against the transport through Drake Passage from eight of the experiments listed in section 2. All of the cases shown have the standard ocean model parameter values and wind stress forcings that are realistic. Figure 15 shows that there is a very strong positive correlation between Drake Passage transport and the strength of the thermohaline circulation off Antarctica. This strong correlation covers a very large range, because the Drake Passage transport varies between 117 Sv in case B and 250 Sv in case C.

In experiments with an active sea-ice model, the strength of the thermohaline circulation off Antarctica is mostly set by the rate of brine rejection into the ocean due to sea-ice formation. This is illustrated by Figure 9 of *Weatherly et al.* [1998], which shows that in cases C and E the rate of Southern Hemisphere ice formation, transport toward lower latitudes, and subsequent melting rate is ~ 4 times the rate estimated from satellite observations. It should also be noted that case K, with the correct air to sea-ice drag coefficient, has a much weaker thermohaline circulation than cases C-E, which all had the air to sea-ice drag coefficient 4 times too large. Figure 16 is a plot of the total buoyancy loss in the ocean due to brine rejection against the Drake Passage transport from the five experiments with an active sea-ice model and the best estimates from observations. There is a very strong positive correlation between the two variables, and the four experiments with stronger than observed buoyancy loss all have larger than observed Drake Passage transports. In experiment L the brine rejection due to sea-ice formation was turned off, and the Drake Passage transport of 122 Sv is the only one of the five experiments that is smaller than the observational value for our choice of model parameters.

6. Discussion and Conclusions

Figure 11 shows that the Drake Passage transport is not set by the Sverdrup transport at the latitude of Cape Horn. There are two reasons why this zonally bounded basin theory does not work for the ACC. The first is that the Sverdrup transport is an estimate of the southward flow across 55°S between Cape Horn and South Georgia at ~ 40°W. This southward flow must be returned by the Malvinas Current, which flows northward between Cape Horn and South Georgia. In the model the Malvinas Current transport need not be the same as the Drake Passage transport. In fact, in experiments C, D, E, H, and K, not all the flow through Drake Passage turns north as the Malvinas Current. For case H this can be seen in Figure 7, which shows that $\sim$ 50 Sv flows to the south of South Georgia. Note that the experiments where this happens are all cases to the right of the diagonal in Figure 11, and so they are cases with larger than observed Drake Passage transports. In case F, for example, which has a realistic Drake Passage transport, Figure 1 shows that virtually all the transport turns northward to flow as the Malvinas Current.

The second reason is that terms other than the wind stress curl and the βv term are important in the depth-integrated vorticity budget. *Wells and DeCuevas* [1995] analyzed this budget from the FRAM integration and showed that there are considerable difficulties in evaluating the bottom pressure term. However, their Table 2 shows that this bottom pressure term, the nonlinear advection term, and the lateral friction term are not negligible in the budget. We have analyzed experiments F and H in the same way and also find that the bottom pressure term is not negligible. Contributions to this term do tend to cancel across bottom ridges, but this term is not small in zonal integral. The lateral friction term in our model is similar in magnitude to the nonlinear advection term in the FRAM analysis, as expected in a noneddy-resolving model. Thus simple Sverdrup theory does not work for the ACC. We

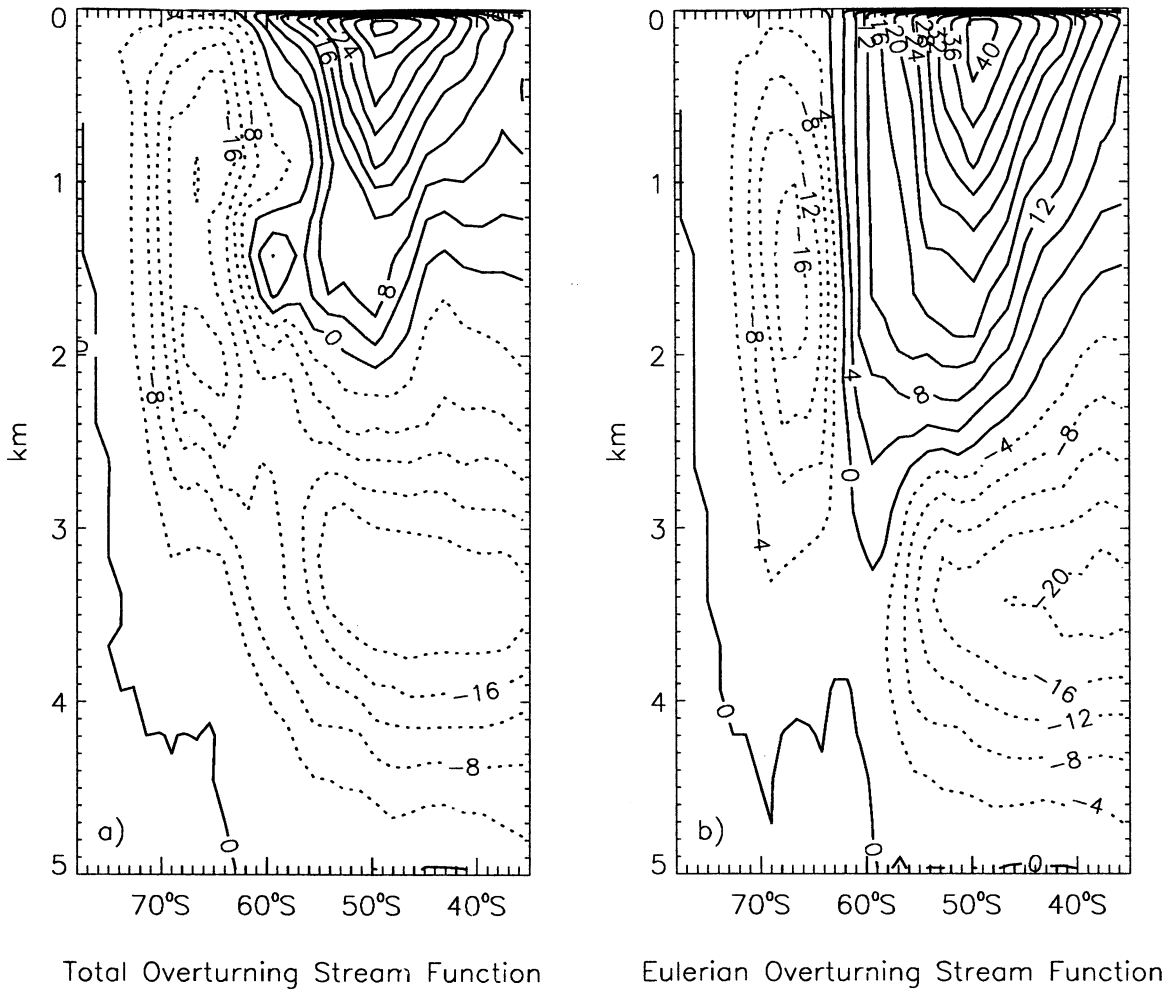

Figure 14. Same as Figure 2, but from the last 5 years of case C, but the contour interval is uniformly 4 Sv.

note that the same conclusion has also been reached by *Ivchenko et al.* [1999, p. 42], who conclude from an equivalent barotropic model based on FRAM, that "the wind stress itself is much more important than its curl, unlike the wind driven circulation in a closed basin," in setting the Drake Passage transport.

Figure 12 shows that the Drake Passage transport is not set by the square root of the meridional Ekman transport, as predicted by the theory of *Johnson and Bryden* [1989]. As noted in the Introduction, the theories discussed there consider only the wind-driven circulation and neglect any effects due to the thermohaline circulation. Our results show a very strong sensitivity of the Drake Passage transport to the strength of the thermohaline circulation off Antarctica. This is consistent with the earlier coarse resolution modeling studies of *Olbers and Wubber* [1991], *Cai and Baines* [1996], and *Gnanadesikan and Hallberg* [2000], which were also described in the introduction.

In our numerical model the mean Drake Passage transport depends on the model parameter values and the setup of topography. An important effect of the latter is to set the intermediate layer, as defined in section 4, which is chosen as realistically as possible for the given vertical resolution. Experiments G, I, and J illustrate the model sensitivity to the parameterized magnitude of eddy activity, the horizontal viscosity, and the background vertical diffusivity, respectively. Experiment G illustrates the largest sensitivity and shows that the ACC transport decreases by 30% when the magnitude of eddy activity is doubled. Despite these sensitivities we believe that our coarse resolution model can be used to give quantitative estimates of what factors set the Drake Passage transport (see the discussions at the end of the Introduction and section 3).

When the model formulation and parameter values are fixed, however, our conclusion is that the Drake Passage transport is set by two external forcing factors. The first is the strength of the meridional Ekman transport at the latitude of Drake Passage, and the second is the strength of the thermohaline circulation off the Antarctic shelf. Figures 10 and 14 show that when the two external forcing factors increase, some of the increased northward transport in the Ekman and deep

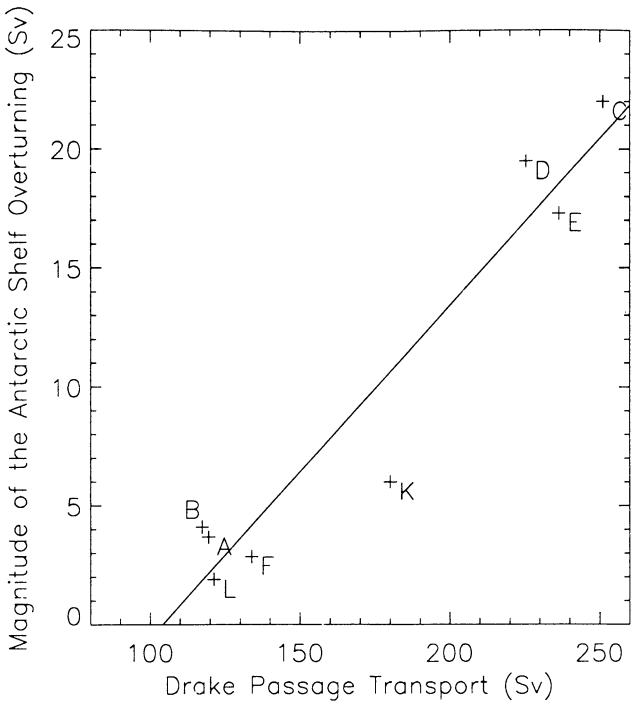

Figure 15. Magnitude of the total meridional overturning off the Antarctic shelf (in Sv) against Drake Passage transport (in Sv) from eight of the model experiments.

layers, respectively, at the latitude of Drake Passage, is returned southward in the intermediate layer, between 400 m and 2.3 km. Figure 13 shows that this relationship is monotonic but not necessarily linear. The reason is that the fraction of the increased northward transport returned in the intermediate layer is not constant, and the remainder is returned southward in the deep layer below the depth of the highest topography.

The intermediate layer is defined in section 4, and in this depth range the effects of vertical stress and the pressure term are negligible. Thus an increase in southward flow will cause an increase in the Coriolis term, which will initially accelerate the eastward zonal velocity. This will result in a stronger ACC and Drake Passage transport. In our model the acceleration stops when the meridional divergence of the Reynolds stress increases sufficiently to balance the Coriolis term. To be effective in strengthening the ACC, the stronger southward velocity must occur in the intermediate layer, because if it occurs in the deep layer, it can be easily balanced by an increase in the pressure differences across the bottom ridges. Another reason that the intermediate layer is the most effective at accelerating the ACC is that the dominant terms are much smaller in that layer than in the Ekman and deep layers (see Figures 9 and 10). Hence a small increase in southward velocity causes an increase in the strength of the ACC. The thickness of the intermediate layer would, in fact, be greater if the integral were not taken zonally but, instead, along the axis of the ACC. The reason is that the ACC avoids the tallest topography at the Drake Passage latitude, which is the South Sandwich Islands. The tallest topography along the axis of the ACC is probably Drake Passage itself, at ~ 3 km. Thus the intermediate layer along the axis of the ACC probably reaches from ~ 400 m down to ~ 3 km.

Figures 15 and 16 show that cases C-E with much too strong Drake Passage transports also have much too strong thermohaline circulations and brine rejection into the ocean because of sea-ice formation. Figure 15 shows that the Drake Passage transport is very sensitive to the magnitude of the overturning off Antarctica. A straight line, least squares fit to the data in Figure 15 has a slope of 0.14 and intersects the abscissa at a value of 104 Sv. This suggests that an increase in the thermohaline overturning off the Antarctic shelf of 1 Sv produces about a 7 Sv increase in Drake Passage transport. This indicates that, in our model, if there were no overturning off the Antarctic shelf, then the Drake Passage transport would be ~ 100 Sv. If this result can be applied to the real ocean, it indicates that ~ 100 Sv of the Drake Passage transport results from the meridional Ekman transport at the latitude of Drake Passage and ~ 30 Sv is due to the thermohaline circulation off the Antarctic shelf.

Acknowledgments. We would like to thank Bruce Briegleb, Gokhan Danabasoglu, Matthew Hecht, and Stephen Yeager, who set up, ran, and analyzed the experiments discussed in this paper. The National Center for Atmospheric Research is sponsored by the National Science Foundation. Stephen Yeager is funded in part by a cooperative agreement from the National Oceanic and Atmospheric Administration.

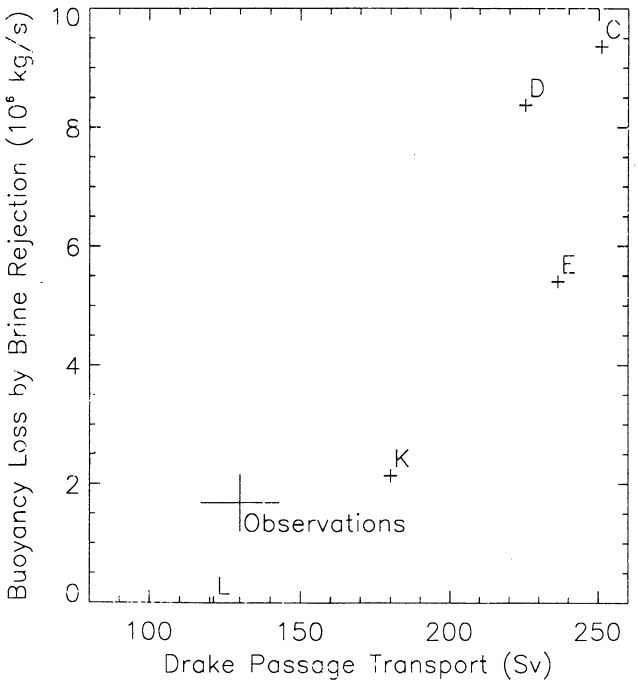

Figure 16. Total buoyancy loss due to brine rejection (in 10^6 kg s^{-1}) against Drake Passage transport (in Sv) from observations and the five experiments with an active sea-ice model.

References

Boville, B. A., and P. R. Gent, The NCAR climate system model, version one, *J. Clim.*, *11*, 1115-1130, 1998.

Bryan, F. O., Climate drift in a multi-century integration of the NCAR Climate System Model, *J. Clim.*, *11*, 1455–1471, 1998.

Bryan, K., Accelerating the convergence to equilibrium of ocean-climate models, *J. Phys. Oceanogr.*, *14*, 666–673, 1984.

Cai, W., and P. G. Baines, Interactions between thermohaline and wind driven circulations and their relevance to the dynamics of the Antarctic Circumpolar Current in a coarse resolution global ocean general circulation model, *J. Geophys. Res.*, *101*, 14,073-14,093, 1996.

Danabasoglu, G., On the wind-driven circulation of the uncoupled and coupled NCAR climate system ocean model, *J. Clim.*, *11*, 1442–1454, 1998.

Danabasoglu, G., and J. C. McWilliams, Sensitivity of the global ocean circulation to parameterizations of mesoscale tracer transports, *J. Clim.*, *8*, 2967–2987, 1995.

Danabasoglu, G., J. C. McWilliams, and P. R. Gent, The role of mesoscale tracer transports in the global ocean circulation, *Science*, *264*, 1123-1126, 1994.

Danabasoglu, G., J. C. McWilliams, and W. G. Large, Approach to equilibrium in accelerated global oceanic models, *J. Clim.*, *9*, 1092–1110, 1996.

Doney, S. C., W. G. Large, and F. O. Bryan, Surface ocean fluxes and water mass transformation rates in the coupled NCAR Climate System Model, *J. Clim.*, *11*, 1420–1441, 1998.

Doos, K., and D. J. Webb, The Deacon cell and other meridional cells of the southern ocean, *J. Phys. Oceanogr.*, *24*, 429-442, 1994.

Fung, I.Y., D.E. Harrison, and A.A. Lacis, On the variability of the net long-wave radiation at the ocean surface, *Rev. Geophys.*, *22*, 177-193, 1984.

Gent, P. R., and J. C. McWilliams, Isopycnal mixing in ocean circulation models, *J. Phys. Oceanogr.*, *20*, 150–155, 1990.

Gent, P. R., J. Willebrand, T. J. McDougall, and J. C. McWilliams, Parameterizing eddy-induced tracer transports in ocean circulation models, *J. Phys. Oceanogr.*, *25*, 463–474, 1995.

Gent, P. R., F. O. Bryan, G. Danabasoglu, S. C. Doney, W. R Holland, W. G. Large, and J. C. McWilliams, The NCAR climate system model global ocean component, *J. Clim.*, *11*, 1287-1306, 1998.

Gnanadesikan, A., and R. W. Hallberg, On the relationship of the circumpolar current to southern hemisphere winds in coarse resolution ocean models, *J. Phys. Oceanogr.*, in press, 2000.

Holland, W. R., J. C. Chow, and F. O. Bryan, Application of a third-order upwind scheme in the NCAR ocean model, *J. Clim.*, *11*, 1487–1493, 1998.

Hughes, C. W., Comments on "On the obscurantist physics of form drag in theorizing about the Circumpolar Current," *J. Phys. Oceanogr.*, *27*, 209-210, 1997.

Hughes, C. W., and P. D. Killworth, Effects of bottom topography in the large scale circulation of the southern ocean, *J. Phys. Oceanogr.*, *25*, 2485-2497, 1995.

Hughes, C. W., M. P. Meridith, and K. J. Heywood, Wind driven transport through Drake Passage: A southern mode, *J. Phys. Oceanogr.*, *29*, 1971-1992, 1999.

Ivchenko, V. O., A. E. Krupitsky, V. M. Kamenkovich, and N. C. Wells, Modeling the Antarctic Circumpolar Current: A comparison of FRAM and equivalent barotropic model results, *J. Mar. Res.*, *57*, 29-45, 1999.

Johnson, G. C., and H. L. Bryden, On the size of the Antarctic Circumpolar Current, *Deep Sea Res., Part A*, *36*, 39-53, 1989.

Killworth, P. D., and M. M. Nanneh, Isopycnal momentum budget of the Antarctic Circumpolar Current in the Fine Resolution Antarctic Model, *J. Phys. Oceanogr.*, *24*, 1203-1224, 1994.

Krupitsky, A., and M. A. Cane, On topographic pressure drag in a zonal channel, *J. Mar. Res.*, *52*, 1-22, 1994.

Krupitsky, A., V. M. Kamenkovich, N. Naik, and M. A. Cane, A linear equivalent barotropic model of the Antarctic Circumpolar Current with realistic coastlines and bottom topography, *J. Phys. Oceanogr.*, *26*, 1803-1824, 1996.

Large, W. G., J. C. McWilliams, and S. C. Doney, Oceanic vertical mixing: A review and a model with a nonlocal boundary layer parameterization, *Rev. of Geophys.*, *32*, 363-403, 1994.

Large, W.G., G. Danabasoglu, S.C. Doney, and J.C. McWilliams, Sensitivity to surface forcing and boundary layer mixing in the NCAR CSM ocean model: Annual–mean climatology, *J. Phys. Oceanogr.*, *27*, 2418–2447, 1997.

Large, W.G., G. Danabasoglu, J.C. McWilliams, P. R. Gent, and F. O. Bryan, Equatorial circulation of a global ocean climate model with anisotropic horizontal viscosity, *J. Phys. Oceanogr.*, in press, 2000.

Munk, W. H., and E. Palmen, Note on the dynamics of the Antarctic Circumpolar Current, *Tellus*, *3*, 53-55, 1951.

Olbers, D., Comments on "On the obscurantist physics of form drag in theorizing about the Circumpolar Current," *J. Phys. Oceanogr.*, *28*, 1647-1654, 1998.

Olbers, D., and C. Volker, Steady states and variability in oceanic zonal flows, in *Decadal Climate Variability*, edited by D. L. T. Anderson and J. Willebrand, NATO ASI Ser. I, *44*, 407-433, 1996.

Olbers, D., and C. Wubber, The role of wind and buoyancy forcing of the Antarctic Circumpolar Current, in *Strategies for Future Climate Research*, edited by M. Latif, pp. 161-191, Max Planck Institut fur Meteorologie, Hamburg, Germany, 1991.

Shea, D. J., K. E. Trenberth, and R. W. Reynolds, A global monthly sea surface temperature climatology, NCAR Tech. Note NCAR/TN-345, 167pp. 1990.

Stommel, H., A survey of ocean current theory, *Deep Sea Res.*, *4*, 149-184, 1957.

Toggweiler, J. R., and B. Samuels, Effect of Drake Passage on the global thermohaline circulation, *Deep Sea Res.*, *42*, 477-500, 1995.

Toggweiler, J. R., and B. Samuels, On the ocean's large-scale circulation near the limit of no vertical mixing, *J. Phys. Oceanogr.*, *28*, 1832-1852, 1998.

Volker, C., Momentum balance in zonal flows and resonance of baroclinic Rossby waves, *J. Phys. Oceanogr.*, *29*, 1666-1681, 1999.

Wajsowicz, R. C., A consistent formulation of the anisotropic stress tensor for use in models of the large scale ocean circulation, *J. Comput. Phys.*, *105*, 333–338, 1993.

Warren, B. A., J. H. LaCasce, and P. E. Robbins, On the obscurantist physics of form drag in theorizing about the Circumpolar Current, *J. Phys. Oceanogr.*, *26*, 2297-2301, 1996.

Weatherly, J., B. Briegleb, W. G. Large, and J. Maslanik, Sea ice and polar climate in the NCAR CSM, *J. Clim.*, *11*, 1472–1486, 1998.

Webb, D. J., A simple model of the effect of the Kerguelen Plateau on the strength of the Antarctic Circumpolar Current, *Geophys. Astrophys. Fluid Dyn.*, *70*, 57-84, 1993.

Webb, D. J., The vertical advection of momentum in Bryan–Cox–Semtner ocean general circulation models, *J. Phys. Oceanogr.*, *25*, 3186–3195, 1995.

Wells, N. C., and B. A. DeCuevas, Depth-integrated vorticity budget of the Southern Ocean from a general circulation models, *J. Phys. Oceanogr.*, *25*, 2569-2582, 1995.

Whitworth, T., Monitoring the transport of the Antarctic Circumpolar Current in Drake Passage, *J. Phys. Oceanogr.*, *13*, 2045-2057, 1983.

Whitworth, T., W. D. Nowlin, and S. J. Worley, The net transport of the Antarctic Circumpolar Current through Drake Passage, *J. Phys. Oceanogr.*, *12*, 960-971, 1982.

Zhang, J., and W. D. Hibler, On an efficient numerical method for modeling sea ice dynamics, *J. Geophys. Res.*, *102*, 8691-8702, 1997.

F. O. Bryan, P. R. Gent, and W. G. Large, National Center for Atmospheric Research, P.O. Box 3000, Boulder, CO 80307 (gent@ucar.edu)

(Received April 29, 1999; revised February 3, 2000; accepted February 7, 2000.)